J. Fluid Mech. (2006), *vol.* 567, *pp.* 281–297.
doi:10.1017/S0022112006002278 Printed in the United Kingdom

Structures of separation on a circular cylinder in periodic flow

By TURGUT SARPKAYA

Department of Mechanical and Astronautical Engineering, Naval Postgraduate School, Monterey, CA 93943, USA

(Received 7 February 2006 and in revised form 8 May 2006)

The structures of separation on a smooth circular cylinder immersed in a sinusoidally oscillating flow are examined in detail for a constant value of the frequency parameter β as the Keulegan–Carpenter number K is systematically increased from the marginally stable to fully separated region in the (K, β)-plane. The positions of the separation points are measured using sublayer fences, flush-mounted hot-film sensors, and extensive high-speed video recordings. The variations of the length scales of the resulting structures, the irregularity of the dye concentration fields, and measurements with two sensors have shown that the separation is three-dimensional, time-dependent, often turbulent, and far from being an eruption of a double-sided single shear layer, or a self-contained bubble. The increase of the three-dimensionality of the flow, evolution of various sizes of structures, secondary separations within the primary separation zone, and the occasional eruption of multiple shear layers are quite similar to the first direct numerical simulation of a laminar separation bubble in the presence of an oscillating inlet flow.

1. Introduction

Separation is a fundamental unsolved phenomenon in modern fluid dynamics and the numerical and experimental study of its occurrence in both steady and unsteady ambient flow about bluff bodies is of paramount importance. A classical example of an unsteady moving separation is that which occurs on a smooth circular cylinder immersed in a sinusoidally oscillating flow, defined here by $u(t) = -U_m \cos(2\pi t/T)$, where U_m is the maximum velocity in the cycle and T is the period of oscillation.

The structure of separation depends primarily on the Keulegan–Carpenter (1956) number $K = 2\pi A/D = U_m T/D$, where A is the amplitude of the relative motion and D is the diameter of the cylinder, and the frequency parameter $\beta = fD^2/\nu = Re/K$, where $f(=1/T)$ is the frequency of the flow oscillation, $Re = U_m D/\nu$ and ν the kinematic viscosity of the fluid. Schlichting (1932, 1979) was the first to show that the ratio of the convective acceleration to local acceleration in a one-dimensional flow is proportional to $U_m T/D$ or to A/D. Thus, a flow with a relatively small K is said to be inertia dominated and a flow with a relatively large K is said to be drag dominated (Sarpkaya 1986).

Aside from its intrinsic interest, the subject is of practical importance in many fields of engineering. In fact, the forces exerted on bodies subjected to vortex-excited oscillations (Sarpkaya 2004) and to the springing and ringing response of compliant systems require a clear understanding of the flow in the range of Keulegan–Carpenter numbers from about 10^{-3} to 10 and frequency parameters from about 1 to 10^8.

There are at present no known predictions of the drag and inertia forces exerted on slender structures undergoing excitation, save for those at K values smaller than about 2 and β values smaller than about 1000 where the classical solution of Stokes (1851) for unseparated laminar flow holds true. Furthermore, the (K, β)-plane contains unexpected phenomena such acoustic streaming (Schlichting 1932; Riley 1975; Lighthill 1978), Honji instability (Honji 1981), dipole tubes, quasi-coherent structures, and transition to turbulence, at least during part of the cycle (Sarpkaya 1993, 2002). In other words, every possible combination of K and β is of practical as well as theoretical importance and touches all aspects of time-dependent flows. However, the difficulties encountered in separating very small drag forces from the large inertial forces and the extreme difficulties encountered in experiments and three-dimensional numerical simulations remain as challenging as ever.

There are only a few numerical simulations relevant to our experiments, i.e. the structures of unsteady separation in unsteady ambient flow. However, numerous contributions have been made to the simulation of the wakes of bluff bodies in time-dependent flows. We will mention here only a few of the most representative contributions. Dütsch *et al.* (1998) conducted time-averaged LDA measurements and numerical simulations of the laminar flow induced by the harmonic in-line oscillations of a circular cylinder in water at rest for (Re, K): (100, 5), (200, 10), and (210, 6) and confirmed that both flow field and force coefficients can be reliably predicted by numerical simulations, at least within the range of their parameter space. Even though they have not discussed the details of the flow in the vicinity of the mobile separation points, they have noted that an upper and a lower boundary layer flow developed as the oscillating cylinder moved in the forward direction and separated at the same upper and lower position on the cylinder wall. The separating flow produced two counter-rotating vortices of apparently the same magnitude of strength. There was no separation at the front and rear stagnation points. As will be discussed in more detail below, our sublayer fences and flush-mounted hot-film sensors revealed no separation at $\theta = 0$ and $\theta = \pi$ (the stagnation points) at any time.

To the best of our knowledge, there are no experiments which deal with separations within a separation bubble. Justesen (1991) computed the separation angle with respect to phase on a cylinder subjected to sinusoidally oscillating laminar flow ($\beta = 196$), assuming that the flow remains two-dimensional and the separation occurs where the wall shear vanishes. According to the MRS criterion (Moore 1957; Rott 1956; Sears 1956), it is the simultaneous vanishing of the shear and the velocity at a point within the boundary layer that determines the separation point. However, the proposed 'criterion' is extremely difficult to apply because it requires *a priori* knowledge of the separation speed (see e.g. Williams 1977) in addition to assuming that there is only one separation point while, in fact, there can be several simultaneously occurring separations at a given time, as demonstrated in this paper. Dong & Karniadakis (2005) advanced the state of the art of direct numerical simulation (DNS) to Reynolds numbers as high as 10 000 for turbulent flows past stationary and oscillating circular cylinders. Their emphasis was placed on the influence of the cylinder oscillation on the physical quantities, such as the drag and lift coefficients. Comparisons with the available experimental data have shown that the simulation has captured the physical quantities reasonably well. However, the details of flow in the vicinity of the mobile separation points were not elucidated. Elston, Blackburn & Sheridan (2006) investigated the oscillatory flow past a stationary cylinder at low K ($\in$ [0, 10]) and β ($\in$ [0, 100]) values using Floquet analysis and direct numerical simulation. They have shown that there are two fundamentally different types of symmetry-breaking

instability within this range: two-dimensional and three-dimensional. There is also a direct primary breakup to three-dimensional instability at frequency parameters β larger than about 50. This is like the 'bypass transition' (Morkovin 1993) in steady flow over a flat plate without the appearance of Tollmien–Schlichting waves 'when the external mainstream initially contains rotational motion either in the form of mainstream turbulence or discrete identifiable vortex motions' (Smith & Walker 1995). Elston *et al.* (2006) also noted that 'On the basis of Sarpkaya's results (2002), it further appears that for all β larger than about 50 this mode remains the first to be encountered as Keulegan–Carpenter numbers are increased from small values'. Authoritative descriptions of flow around circular cylinders with emphasis on fundamentals, applications, and time-dependent flows are given by Zdravkovich (1997, 2003, 2006) in his monumental work and we can do no better than to refer to that for additional inspiration.

A definition of separation that is applicable to all kinds of flows has not yet been established. Taneda (1980) argued that the departure of dye filaments from the surface is the most useful definition of separation for most time-dependent flows. This definition coincides with the Prandtl criterion in the case of two-dimensional flow over a fixed wall, and the flow separation can be detected only by observing the integrated streaksheet. According to Van Dommelen & Shen (1982) and Walker (2003), it is the abrupt eruption of a 'double-sided shear layer' and the expelling of concentrated vorticity into the external flow. However, the numerical simulation of narrow eruptive spires in turbulent shear flows is beyond the scope of even the current spectral methods (Brinckman & Walker 2001).

In sinusoidally oscillating flows, as in the case under consideration, the shear layers undergo rapid transition to turbulence and the position of transition moves back and forth on the crowns of the cylinder (without wake reversal for K smaller than about 5). The theoretical and experimental treatment of the boundary layers with wake return is even more difficult, particularly when the state of the boundary layer changes during a given cycle. An in-depth discussion of these is presented by Haller (2004) and will not be repeated here. Suffice it to note that, recently, Kilic, Haller & Neishtadt (2005) used the method of averaging to improve separation criteria for two-dimensional unsteady flows with a well-defined asymptotic mean velocity. However, they have concluded that, 'the application of averaging methods to moving unsteady separation remains an open question. In moving separation, the location of the separation point changes in time, and hence will not be captured by averaging over infinite times'.

For the periodic flow over a circular cylinder, the minimum value of K at which separation occurs has not yet been determined, owing to a number of difficulties associated with computational and experimental limitations. It appears that it is strongly dependent on K and β and the manner in which the observations are made, i.e. the inception and visibility of separation do not occur simultaneously. Regarding the structures of separation, the most relevant to our investigation and, in fact, the first work to report results of the DNS of a laminar separation bubble in the presence of an oscillating inlet flow is that by Wissink & Rodi (2003). Their computational domain consisted of a no-slip flat plate at the lower wall and a free-slip boundary, similar in shape to the upper half of a two-dimensional Venturi meter. Their Reynolds number, based on U_o and a length scale L (proportional to the length of the flat plate), was $Re = 60\,000$. They have presented a sequence of snapshots, showing the contours of the magnitude of the instantaneous vorticity along the wall normal. These have shown the evolution of strong dipoles that propelled themselves and broke through the

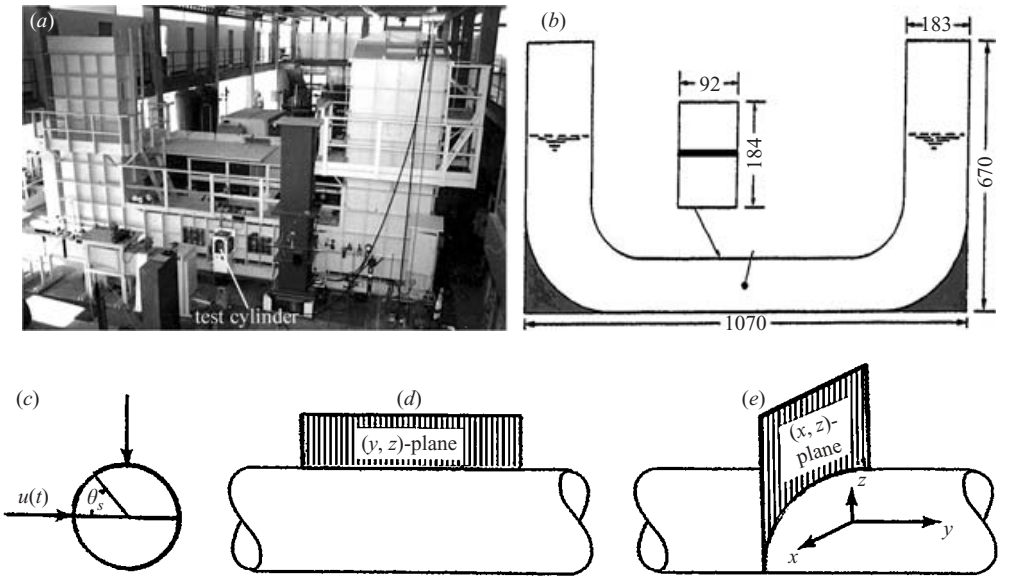

FIGURE 1. (*a*) A photograph and (*b*) a schematic drawing of the U-shaped water tunnel (all dimensions are in cm). The tall square structure in the foreground (left) is the filtration system. The working section is 148 cm high, 92 cm wide, and 10.7 m long. The two 6.7 m vertical sections are each 183 cm wide by 92 cm long. (*c*) The separation angle, (*d*) the planes of the laser light sheets, and (*e*) the coordinate axes.

original shear layer. This was considered as the precursor of the shedding of a roll of turbulent flow. In addition to the dipoles, relatively small entrained instabilities were found to grow very quickly and many three-dimensional vortical structures appeared inside the separation region. These are, indeed, very similar to our observations to be described in detail in the next section and demonstrate the value of numerical models in providing additional insight into the physical mechanisms driving the separation process.

2. Data acquisition

The experiments were conducted in a large U-shaped water tunnel where the flow oscillated about a smooth cylinder ($D = 184$ mm) at a constant resonant frequency of $f = 0.187$ Hz. Figure 1(*a–e*) shows the image and the schematic drawing of the tunnel, the definition of the separation angle, the positioning of the laser light sheets, and the coordinate axes. The selection of D was based on minimizing the unavoidable wall effects, limiting K to values smaller than about 5, and maximizing the Reynolds number. The exploratory experiments with a smooth cylinder of $D = 5.08$ cm ($L/D = 12$) vibrating at ($K = 3.45$, $\beta = 520$, $Re = 2000$), in a different glass-sided water tank (Sarpkaya 1986), exhibited only mildly turbulent separations, showing that at relatively small Reynolds numbers the tendency of the flow to break up and to give rise to localized three-dimensional phenomena is considerably reduced.

The spectra of the velocity at various positions in the test section (obtained through the use of a three-dimensional laser-Doppler-velocimeter (LDV) system have shown that the contributions of the second and higher harmonics are indeed negligible. The transient period to reach a constant K from rest varied from six to ten cycles for $K < 1$ and a smaller number of cycle for larger K (Sarpkaya 2002).

The evolution of the structures in the separation region was recorded using two laser light sheets, positioned as shown in figure 1(*c–e*), and a digital video camera (with frame rates from 250 to 8000 frames/s and shutter speeds from 1/60 to 1/10 000 s) for subsequent frame-by-frame analysis. In addition, the motion of the primary and secondary separation fronts on the mid-section of the cylinder was determined as a function of time through the use of six differential-pressure probes (for additional details see Konstantinov & Dragnysh 1955; Rechenberg 1962, 1963; Achenbach 1968, 1971; and Sarpkaya & Butterworth 1992) and six flush-mounted hot-film sensors (see e.g. Mendez & Ramaprian 1985; Eaton *et al.* 1979; Ruderich & Fernholz 1986). The sensors have performed quite satisfactorily at K values smaller than about 8 and yielded separation points remarkably close to those obtained with the differential-pressure probes.

The output of the probes, fences, and other transducers (elevation, velocity, acceleration, temperature, etc.) were sampled at a rate of 720 samples per channel for 50 cycles of flow oscillation for a given angular position of the cylinder. Then the cylinder was rotated (in the clockwise direction) at 5° intervals (with ample time between the rotations to take data), and the procedure was repeated until the first probe has rotated 360°. Then the measurements were repeated by rotating the cylinder in the counterclockwise directional at 5 ° intervals until the first probe returned to its initial position. It is important to note that there were no mode changes in the course of 144 sets of experiments for any K in the range of K values encountered in the experiments. Therefore, there was no need to use a conditional sampling scheme to identify and separate the prevailing flow modes. Additional details of the equipment and procedures are given in Sarpkaya (1977, 1993, 2002).

Normally, the amplitude of oscillations and hence K are changed from one value to another by enlarging or constricting a two-dimensional orifice in the pneumatic system. For the present experiments, however, a particular K was set up in the tunnel either by gradually increasing the prevailing K or by starting the flow from rest (after a period of about an hour). The reasons for the two flow-establishment schemes were partly to explore the history effects on the evolution of the flow structures and partly to replenish the fluorescent dye, which dissolved after many cycles of oscillation. Extensive observations and tape recordings with both schemes have shown that the secondary separations did not develop immediately after arriving at a new K value but took about 10 cycles or so to reach a quasi-steady state, i.e. no history effects were observed after about 10 cycles. Evidently, the results of the experiments which depend only on K and β cannot be compared with those which depend on K, β, and $\partial K/\partial t$, as in the case of experiments with a cylinder undergoing damped oscillations.

3. Results and discussion

We have previously established (Sarpkaya 2002) that the (K, β)-plane (see figure 2) may be divided into three regions: a stable region ($K < K_{cr}$) in which there are no structures identifiable by flow visualization, an unstable transition region ($K_{cr} < K < K_h$) in which there are quasi-coherent structures leading to mushroom-shaped coherent structures at $K \approx K_h$, and an increasingly chaotic region ($K > K_h$) where coherent structures undergo complex interactions, eventually leading to separation and turbulence. The two boundaries defined by $K = K_{cr}$ and $K = K_h$ (after Hall 1984) are not sharp demarcation lines. They should be regarded as narrow fuzzy bands whose extent depends on observers' ability to interpret 'small disturbances' and nearly 'perfect' mushrooms in laboratory experiments. We describe here only

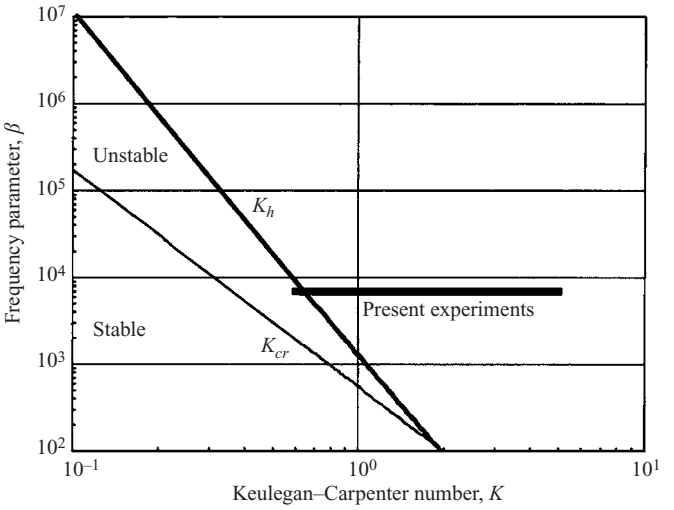

FIGURE 2. The (K, β) stability map (from Sarpkaya 2002). The horizontal solid line shows the range of the present experiments.

the evolution of the structures for $\beta = 6815$ as K is systematically increased from $K_h \approx 0.6$ to about 5, i.e. as the Reynolds number varies from about 4000 to 34 000. The use of a relatively small K at sufficiently large Reynolds numbers simplifies the observations and measurements (with sublayer fences and flush-mounted hot-film sensors) primarily because the wake remains essentially symmetrical with respect to the horizontal plane passing through the axis of the cylinder in the direction of the ambient flow for K less than about 5.

In the following, the ambient flow is in the x-direction (left to right) in the interval $0.25 < t/T < 0.75$ and negative in the interval $0.75 < t/T < 1.25$. The axes y and z are in the lateral (along the axis of the cylinder) and vertical directions, respectively. Figure 3(a), for a light sheet in the (y, z)-plane, shows the side views of three vortex tubes in the vicinity of the crown of the cylinder for $K_h = 0.65$. It is representative of relatively smooth mushrooms in the interval $0.60 < K < 1.2$. The structures are spaced by about 21 mm and the lateral dimension of the oval is about 9 mm and the vertical dimension is about 6 mm. They are taken with a Yag laser pulsing at 32 ms intervals for periods of 7 ns. The mushrooms or dipoles are not perfectly stable structures even at $K = K_h$ and there is considerable interaction between them on either side of the Hall line, as evidenced by their deformation (as in figure 3b) and occasional merging (as in figure 3c).

For K slightly larger than 1.2 or Re larger than about 8200 (depending on the character of the random disturbances), the vortex tubes (dipoles) shown in figure 3(a) develop streamwise waves or streaks, as in figures 4(a, b). These grow with K (as in figure 4c), similar to those found in the transition of flow in a boundary layer on a flat plate. With further (small) increases in K (to 1.38), one or more of the tubes develop egg-shaped bulges or aneurisms, as shown in figure 4(d). As might be expected, such bulges occur neither simultaneously nor at the same angular position relative to the crown of the cylinder. Figures 4(e, f) shows the rapid distortion of the adjacent tubes and the expansion of the bulge in the foreground. Figure 4(g) shows highly disturbed but still laminar structures. Finally, in figure 4(h) one can identify the early signs of separation and the narrow eruptive spires as K approaches a value

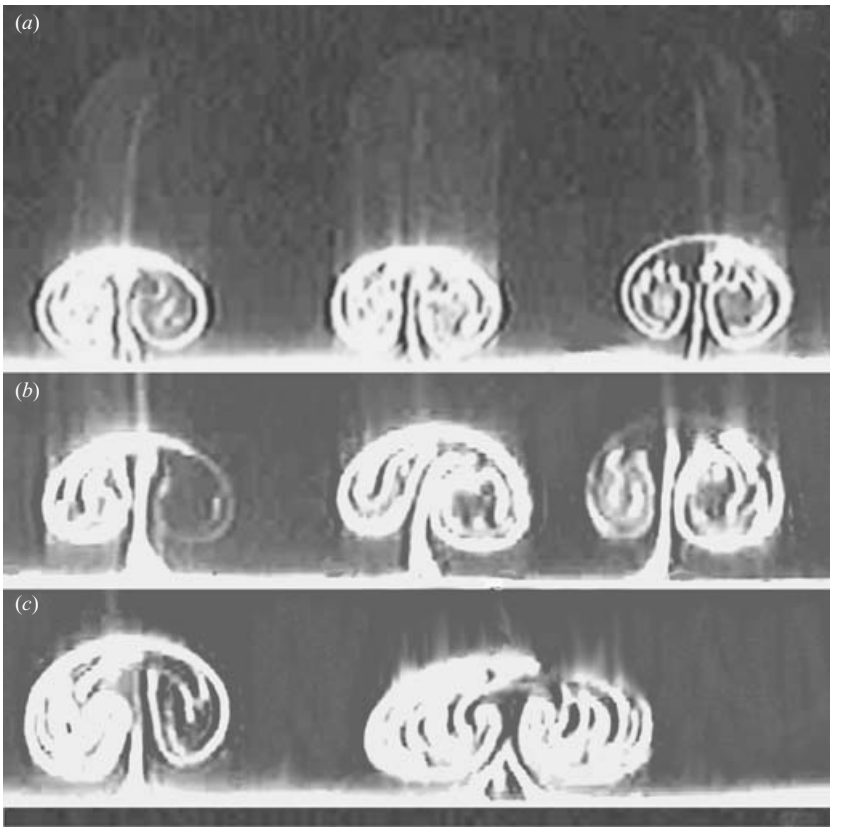

FIGURE 3. (*a*) The cross-sections of three vortex tubes or dipoles in the vicinity of the crown of the cylinder in the (y, z)-plane for $K_h = 0.65$ (on the Hall line). The mushrooms are not perfectly stable even on the Hall line, as evidenced by their deformation as in (*b*) and occasional merging as in (*c*) over a period of about 20 cycles in the course of an uninterrupted run at $K_h = 0.65$.

somewhere between 1.5 and 1.7, depending on the disturbances in a particular cycle. However, the flow is still composed of large three-dimensional laminar structures before it enters an 'intermittent' state at larger K. The discussion of the egg-shaped structures (a three-dimensional oval) is deferred to figure 5.

Figure 5(*a*) shows the cross-sections of the dipoles in the (y, z)-plane in the interval $0.70 < K < 1.2$. For a slightly larger K (about 1.4) or Re larger than about 9500, the dipoles become increasingly irregular (figure 5*b*), come closer, and begin to intertwine (figure 5*c*). With further increases in K, some tubes rapidly move towards the top of the adjacent tubes as in figure 5(*d–f*) and undergo core bursting or some form of vortex breakdown, described in detail in Sarpkaya (1971, 1995). The side views of such breakdowns appear like egg-shaped bulges, as in figure 4(*d–f*). As K approaches a value somewhere between 1.5 and 1.7, the dipole tubes break up into highly complex three-dimensional structures (figure 5*g*). This is followed by the inception of numerous eruptions (figure 5*h*).

The remaining figures show the motion of the separation points (measured from the left stagnation point), and the structure of flow within the separation bubble. Figure 6 is an example of the upstream motion (i.e. to the left) of the separation front in the (x, z)-plane and the evolution of very complex structures in the separation

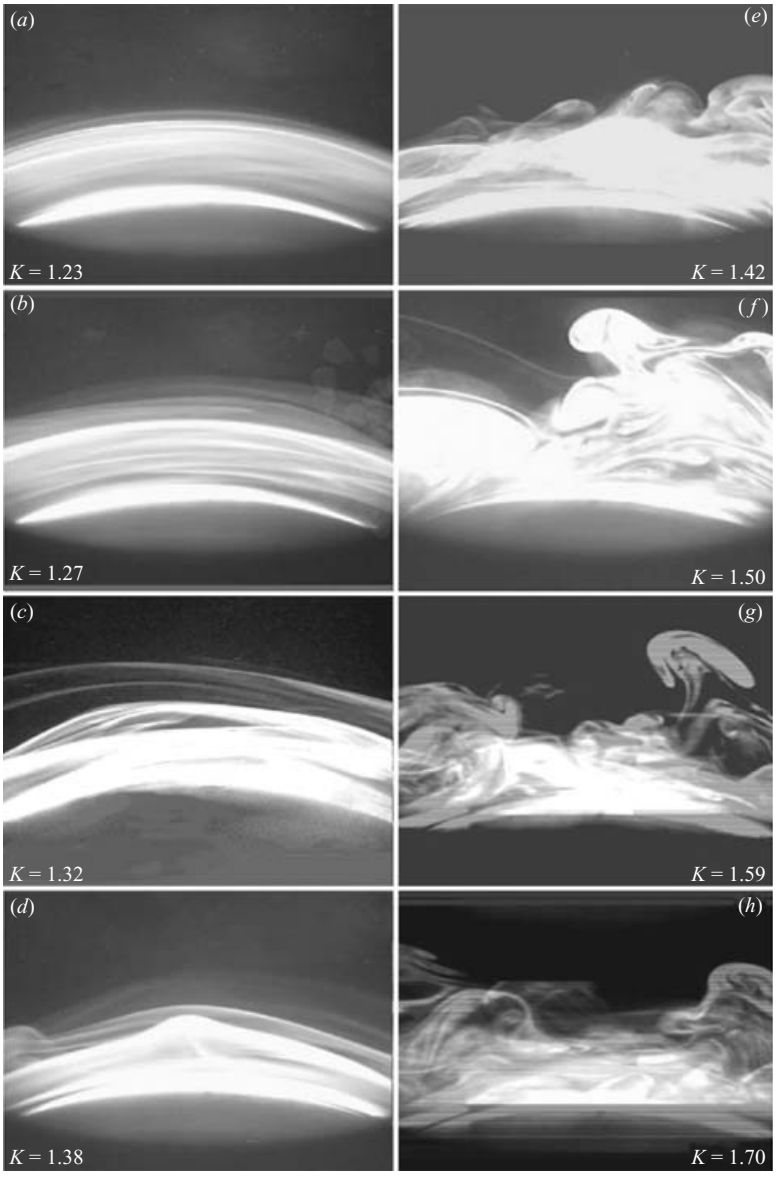

FIGURE 4. The evolution and eventual breakup of the dipole tubes in the (x, z)-plane with increasing K are shown at instant $t/T = 0.25$. The motion of the dipoles for a given K repeats from cycle to cycle with surprising regularity, as seen clearly in high-speed video tapes.

region for $K = 3.45$ ($Re \approx 23\,500$). In general, the pictures show that the separation zone is composed of numerous dipoles and vortical structures of various sizes, which become increasingly three-dimensional. This is compounded by the changes in the velocity and acceleration within as well as outside the separation region. For the case under consideration, the separation which began at $t/T \approx 0.27$ at about $\theta_s = 160^\circ$ moves very rapidly towards the crown of the cylinder in $\Delta(t/T) = 0.08$ (≈ 0.43 s) and reaches $\theta_s = 84^\circ$ at $t/T = 0.35$ (figure 6*a*, filled triangles in figure 7) with a mean $\mathrm{d}\theta_s/\mathrm{d}t \approx 178^\circ\,\mathrm{s}^{-1}$. As the flow continues to accelerate (left to right) in the

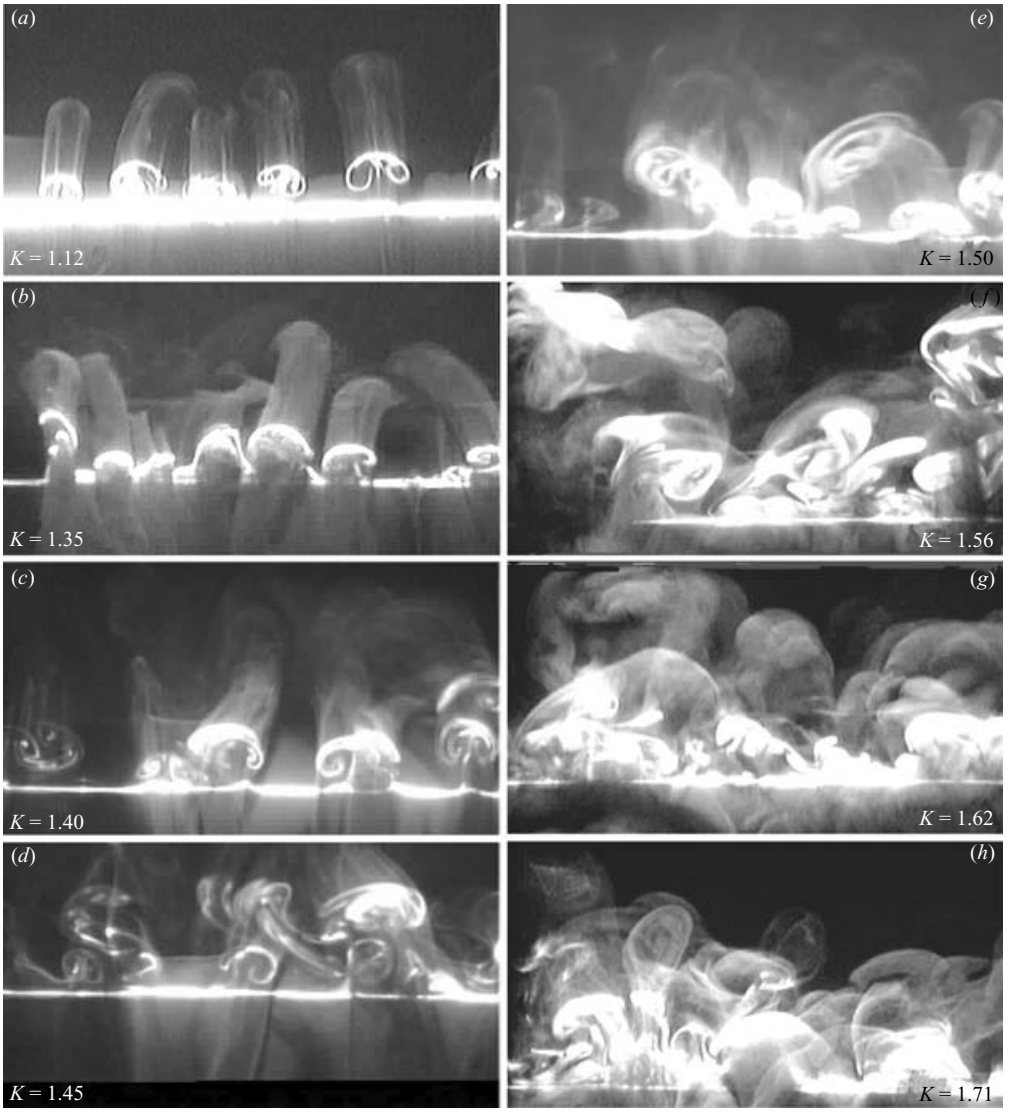

FIGURE 5. Each frame in the (y,z)-plane shows an instant $(t/T = 0.25)$ for a given K. The three-dimensionality of the dynamic system and the surprising regularity of the intertwining motion of the dipoles in each cycle are clearly seen in high-speed video tapes.

time interval $0.25 < t/T < 0.50$, the separation front moves rather slowly to $\theta_s = 81.5^\circ$ at $t/T = 0.40$ (figure 6*b*). The reason for this is that the velocity and acceleration reach 70 % of their maximum values at $t/T = 0.375$ in a direction opposite to that of the motion of the separation point. The front of the separation remains well defined as long as the velocity and acceleration are in the same direction (figure 6*c* (78°, 0.41), figure 6*d* (75°, 0.43), and figure 6*e* (72.5°, 0.44)). As t/T approaches 0.50, as in the case of figure 6(*f*) (64°, 0.49), the velocity nears its maximum, as the acceleration tends to zero. The structures begin to grow rather rapidly in the radial direction, break up into large lumps or turbulent patches (separated by small regions of smooth flow) along the arc of the separation region, and secondary separation sets

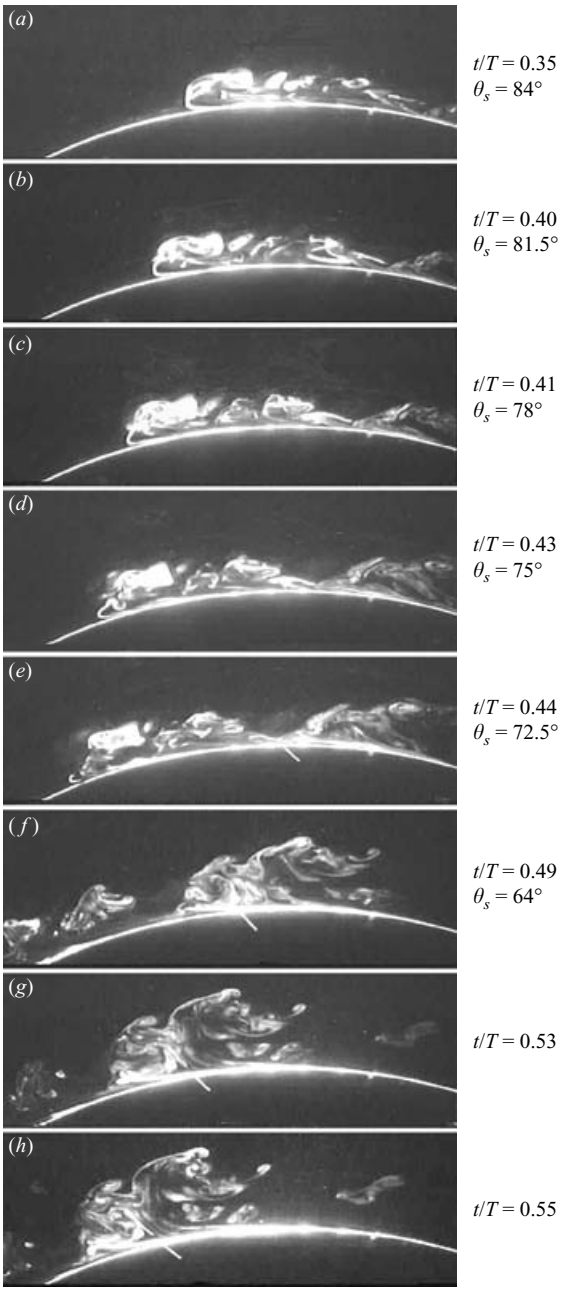

FIGURE 6. Evolution of the structures of separation at eight sequential instants for $K = 3.45$ and $Re = 23\,500$: the times, the separation angles, the breakup of the laminar structures, and the secondary separations (identified by white lines) on the wall (clearly seen in *f*–*h*). The separation angles for (*g*) and (*h*) cannot be determined from the video pictures but they are available in figure 7 from the sublayer fences and hot-film sensors.

in (near the crown of the cylinder as seen in figure 6*f*–*h*). The secondary separations were easily detectable with both hot-film sensors and sublayer fences. However, the hot-film sensors produced sharper signals. The numerical simulations of Wissink & Rodi (2003) exhibited similar structures in their spanwise vorticity snapshots even in

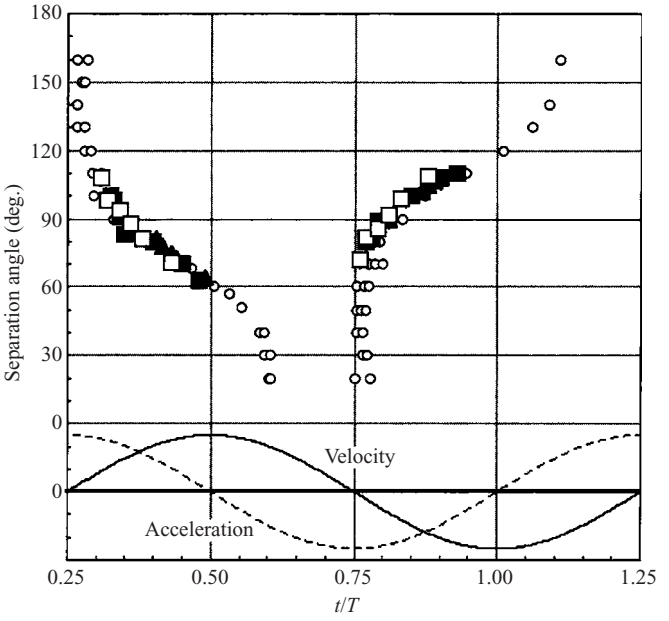

FIGURE 7. Instantaneous separation angles within one period for $K = 3.56$, $Re = 23\,500$ (filled triangles); $K = 3.95$, $Re = 27\,000$ (filled squares); and $K = 4.45$, $Re = 30\,300$ (open squares). Measurements with the differential probes and the flush-mounted hot-film sensors for $K = 3.95$, $Re = 27\,000$ are shown with open circles. No distinction was made between them because of their remarkably close agreement.

a significantly different flow geometry. A similar separation occurs on the lee side of a prolate spheroid (a submarine body) and forms a surface that rolls up into the secondary vortex located underneath the primary vortex (Chesnakas & Simpson 1997; Sarpkaya 1992).

For $t/T \geqslant 0.50$, the ambient flow begins to decelerate and the shape of the separation front, internal structure of the separation region, and its approximate envelope become increasingly irregular. Even though it is possible to see the onset and evolution of the secondary separations in figure 6(*d*, *e*), there is no ambiguity about the occurrence of secondary separations in figure 6(*f*–*h*) and the rapid increase of the vertical extent of the separation region. It is also noted that the brightness of the structures in the latter frames is reduced, partly due to the attenuation of the light in the thicker separation layer and partly due to the faster diffusion of the dye in a region of enhanced mixing. The open symbols in figure 7 denote the separation data obtained through the use of the sublayer fences and flush-mounted hot-film sensors. No distinction was made between them because of their remarkably close agreement.

Figure 8 shows the upstream motion of separation for $K = 3.95$ ($Re \approx 27\,000$). Both the ambient velocity and acceleration are from left to right, as in the case of figure 6. The separation which began at $t/T \approx 0.27$ at about $\theta_s = 160^\circ$ moves rapidly towards the crown of the cylinder in $\Delta\ (t/T) \approx 0.05$ and reaches $\theta_s \approx 108^\circ$ at $t/T \approx 0.31$ (figure 8*a*, filled squares in figure 7). As the flow continues to accelerate (see figure 7) in the time interval $0.25 < t/T < 0.75$, the separation moves to $\theta_s = 100^\circ$ at $t/T = 0.32$ (figure 8*b*). The front of the separation is well-defined and the separation region contains several vortical structures and shows the onset of turbulence. Furthermore, it is evident from the flow structures behind the primary light

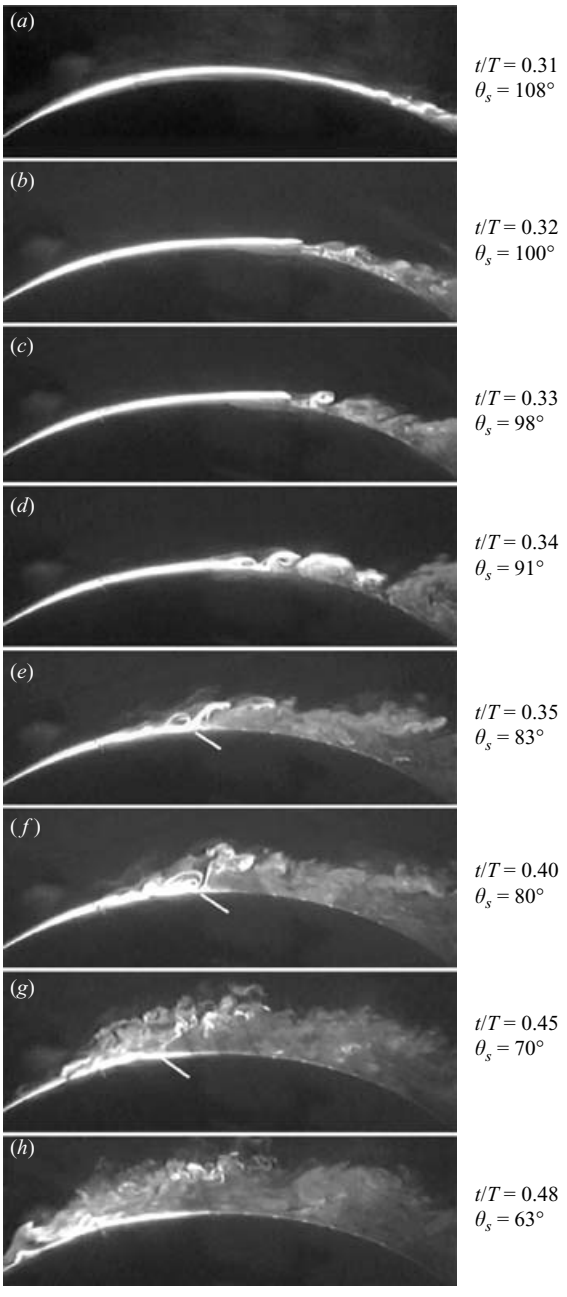

FIGURE 8. The times, separation angles, and the evolution of the structures of separation are shown for $K = 3.95$ and $Re = 27\,000$. Frames (*e*–g) show the eruption of double-sided shear layers (identified by white lines) and the rapid transition to turbulence.

plane that the flow is three dimensional (this is seen clearly in videos). In figure 8(*c*), the separation point is seen to move rather slowly to $\theta_s = 98^\circ$ at $t/T = 0.33$. As noted above, the velocity and acceleration (in the opposite direction to the motion of the separation front) reach 70 % of their maximum values at $t/T = 0.375$, in a direction opposite to that of the motion of the separation point. Thus, it is natural to

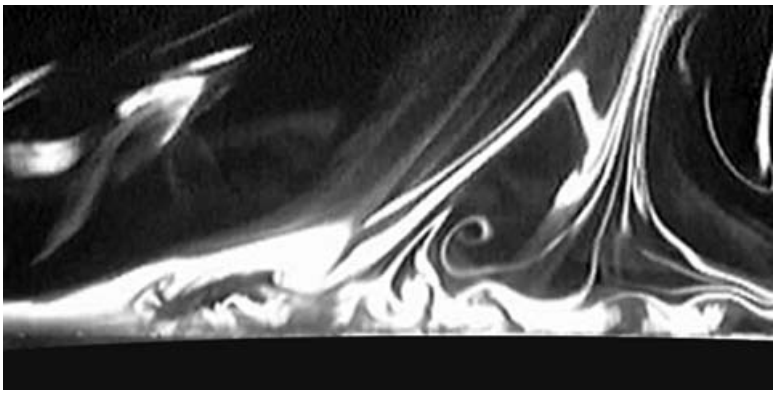

FIGURE 9. A sample moving separation ($K = 3.95$) composed of a number of shear layers (magnified about twenty times). The size of the photographed region is about 3 mm by 1.5 mm. Figure 8(*e*, *f*) exhibits similar separations.

expect the speed of the separation front to slow down. Figures 8(*d*) (91°, 0.34), 8(*e*) (83°, 0.35), 8(*f*) (80°, 0.40), 8(*g*) (70°, 0.45), and 8(*h*) (63°, 0.48) show the evolution of numerous vortical structures, secondary separations, and the intensification of turbulence.

Figures 8(*e–g*) shows the eruption of double-sided shear layers. However, they are somewhat more complicated than the single eruptions seen in steady flows, particularly near their roots or the region of their inception on the boundary. Figure 9 shows for $K = 3.95$ the inception of a sample moving separation composed of a number of shear layers (magnified about twenty times).

Figure 10 shows the upstream motion of separation for $K = 4.45$ ($Re \approx 30\,000$). Both the ambient velocity and acceleration are from left to right, as in the other cases. The separation which began at $t/T \approx 0.27$ at about $\theta_s = 160°$ moves rapidly towards the crown of the cylinder in $\Delta(t/T) \approx 0.04$ and reaches $\theta_s \approx 108°$ at $t/T \approx 0.31$ (figure 10*a*, open squares in figure 7). Unlike the previous cases at lower K, the separated region is now turbulent as evidenced by the intense mixing and rapid diffusion of the dye. It is for the same reasons that the front of the separation region is not as well-defined as in the previous cases. As the flow continues to accelerate (left to right) in the time interval $0.25 < t/T < 0.50$, the separation moves to $\theta_s = 98°$ at $t/T = 0.32$ (figure 10*b*). In figure 10(*c*), the separation point is seen to move rather slowly to $\theta_s = 94°$ at $t/T = 0.34$ where the separation point is clearly defined. The speed of the separation front is slowed down for the reasons noted earlier (U and $\mathrm{d}U/\mathrm{d}t$ being in the opposite direction to the motion of the separation front). Figures 10(*d*) (88°, 0.36), 10(*e*) (81°, 0.38), and 10(*f*) (71°, 0.43) show the evolution of numerous vortical structures, secondary separations, and the intensification of turbulence. In figures 10(*g*) (62°, 0.48) and 10(*h*), the inner separation region is overtaken by the turbulent patches (with larger ambient velocity) directly above them.

Numerous such visualizations have been evaluated at additional K values between 3 and 5. However, the fundamental character of the structures did not differ significantly from those shown in figures 6 ($K = 3.45$, $\beta = 6815$, $Re = 23\,500$), 8 ($K = 3.95$, $\beta = 6815$, $Re = 27\,000$), and 10 ($K = 4.45$, $\beta = 6815$, $Re = 30\,000$). For the experiments reported herein, an observer watching the crown of the cylinder while maintaining K constant sees, in a half-cycle (about 2.7 s), laminar flow, motion of the separation front, and

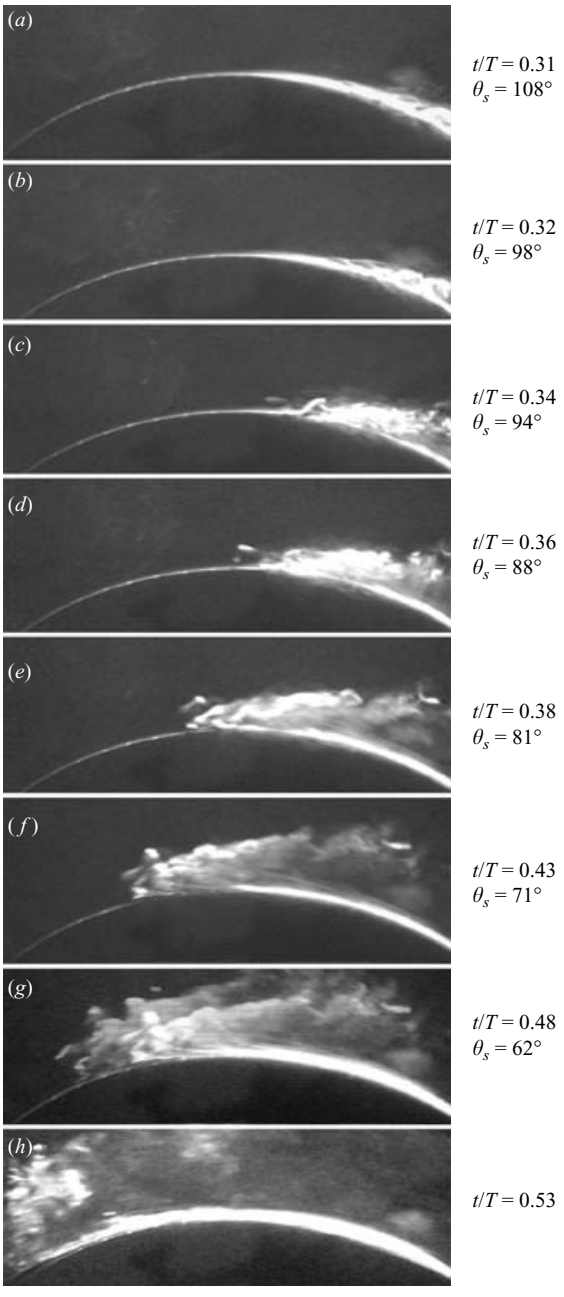

FIGURE 10. The times, separation angles, and the evolution of the structures are shown for $K = 4.45$ and $Re = 30\,300$. It is remarkable that their general forms and angular positions reappear from cycle to cycle even at these K and Re values. The separation angle for (h) cannot be determined from the video pictures but it is available in figure 7 from the sublayer fences and hot-film sensors.

localized three-dimensional phenomena, dependent on K (for a given β), dipoles and laminar patches, the breakup of the coherent structures into smaller and smaller scales (with increasing distance from the separation bubble), secondary separations, and intense mixing leading to three-dimensional fully turbulent flow. Although no

two cycles are exactly alike, or can they be, the basic identifiable characteristics of the separation bubble for a given (K, β) are nearly repeated in the opposite direction in the next 2.7 s, as evidenced by numerous observations, measurements, and video recording at the three K values noted above for $\beta = 6815$. Evidently, separation on a cylinder undergoing sinusoidal oscillations in a fluid otherwise at rest is not a single simple eruption moving along the surface of the cylinder. In fact, in the light of the experiments, one realizes that the separation 'bubble' in an oscillating flow must break up into dipoles and three-dimensional vortical structures, sandwiched between more quiet regions of flow, due to rapidly changing velocity and pressure gradients over the crowns of the cylinder.

4. Concluding remarks

In the range of K values and Reynolds numbers (or β values) encountered in these experiments, the separation is three-dimensional, far from being a single eruption of a double-sided single shear layer or the departure of dye filaments from the surface of a self-contained bubble. The increase of the three-dimensionality of flow, evolution of various sizes of structures, changes of the gradients of velocity, acceleration, and pressure along the moving separation region, secondary separations within the primary separation zone, occasional eruption of multiple shear layers and the enhancement of small-scale structures render the numerical simulation of separation in time-dependent flows a challenge for the distant future. The results presented herein may provide realistic guidance for the modelling as well as the explanation of three-dimensional flow detachment from no-slip curved boundaries.

The work described herein was presented at the IUTAM *Symposium on Unsteady Separated Flows* at the 'Institut Méchanique des Fluids de Toulouse' on April 8–12, 2002. The support of the research program over a period of four years by the National Science Foundation, the Office of Naval Research, and the Naval Postgraduate School is gratefully acknowledged. A special note of thanks is extended to Messrs P. Parker, C. Merrill, and F. Novak for their assistance with the experiments. The comments of the referees are appreciated.

REFERENCES

Achenbach, E. 1968 Distribution of local pressure and skin friction around a circular cylinder in cross-flow up to $Re = 5 \times 10^6$. *J. Fluid Mech.* **34**, 625–639.

Achenbach, E. 1971 Influence of surface roughness and the cross-flow around a circular cylinder. *J. Fluid Mech.* **46**, 321–335.

Brinckman, K. W. & Walker, J. D. A. 2001 Instability in a viscous flow driven by stream wise vortices. *J. Fluid Mech.* **432**, 127–166.

Chesnakas, C. J. & Simpson, R. L. 1997 Detailed investigation of the three-dimensional separation about a 6:1 prolate spheroid. *AIAA J.* **35**, 990–999.

Dong, S. & Karniadakis, G. E. 2005 DNS of flow past a stationary and oscillating cylinder at $Re = 10\,000$. *J. Fluids Struct.* **20**, 519–531.

Dütsch, H., Durst, F., Becker, S. & Lienhart, H. 1998 Low-Reynolds-number flow around an oscillating circular cylinder at low Keulegan–Carpenter numbers. *J. Fluid Mech.* **360**, 249–271.

Eaton, J. K., Jeans, A. H., Ashjaee, J. & Johnson, J. P. 1979 A wall flow direction probe for use in separating and reattaching flows. *Trans. ASME*: *J. Fluids Engng* **101**, 364–366.

Elston, J. R., Blackburn, H. M. & Sheridan, J. 2006 The primary and secondary instabilities of flow generated by an oscillating circular cylinder. *J. Fluid Mech.* **550**, 359–389.

Hall, P. 1984 On the stability of unsteady boundary layer on a cylinder oscillating transversely in a viscous fluid. *J. Fluid Mech.* **146**, 337–367.

Haller, G. 2004 Exact theory of unsteady separation for two-dimensional flows. *J. Fluid Mech.* **512**, 257–311.

Honji, H. 1981 Streaked flow around on oscillating circular cylinder. *J. Fluid Mech.* **107**, 507–520.

Justesen, P. 1991 A numerical study of oscillating flow around a circular cylinder. *J. Fluid Mech.* **222**, 157–196.

Keulegan, G. H. & Carpenter, L. H. 1956 Forces on cylinders and plates in an oscillating fluid. *National Bureau of Stand Rep.* 4821, 5 September 1956. (see also *J. Res. Natl. Bur. Stand.* **60**, 423–440, 1958).

Kilic, M. S., Haller, G. & Neishtadt, A. 2005 Unsteady fluid flow separation by the method of averaging. *Phys. Fluids* **17**, 067104.

Konstantinov, N. I. & Dragnysh, G. L. 1960 The measurement of friction stress at a surface. Department of Scientific and Industrial Research (India) Russian Translation Series.

Lighthill, M. J. 1978 Acoustic streaming. *J. Sound Vib.* **61**, 391–418.

Mendez, A. N. & Ramaprian, B. R. 1985 The use of flush-mounted hot-film gauges to measure skin friction in unsteady boundary layers. *J. Fluid Mech.* **161**, 139–159.

Moore, F. K. 1957 On the separation of the unsteady laminar boundary layer. *Boundary Layers, IUTAM Symposium (Berlin), Freiberg*, pp. 296–311.

Morkovin, M. V. 1993 Bypass-transition research: issues and philosophy. In *Instabilities and Turbulence in Engineering Flows* (ed. D. E. Ashpis, T. B. Gatski & C. Hirsch), pp. 3–30. Kluwer.

Rechenberg, I. 1962 Messung der turbulenten Wandreibung mit dem Prestonrohr. *Jahrbuch der Wissenschaftlichen Gesellschaft für Luft und Raumfahrt e.V.* WGLR.

Rechenberg, I. 1963 Messung der turbulenten Wandschubspannung. *Z. Flugwiss.* **11**, 429–438.

Riley, N. 1975 The steady streaming induced by a vibrating cylinder. *J. Fluid Mech.* **68**, 801–812.

Rott, N. 1956 Diffraction of a Weak shock with vortex generation. *J. Fluid Mech.* **1**, 111–128.

Ruderich, R. & Fernholz, H. H. 1986 An experimental investigation of a turbulent shear flow with separation, reverse flow and reattachment. *J. Fluid Mech.* **163**, 283–322.

Sarpkaya, T. 1971 On stationary and travelling vortex breakdowns. *J. Fluid Mech.* **45**, 545–559.

Sarpkaya, T. 1977 In-line and transverse forces on cylinders in oscillatory flow at high Reynolds numbers. *J. Ship Res.* **21**, 200–216.

Sarpkaya, T. 1986 Force on a circular cylinder in viscous oscillatory flow at low Keulegan–Carpenter numbers. *J. Fluid Mech.* **165**, 61–71.

Sarpkaya, T. 1992 Brief reviews of some time-dependent flows. *Trans. ASME*: *J. Fluids Engng* **114**, 283–298.

Sarpkaya, T. 1993 Coherent structures in oscillatory boundary layers. *J. Fluid Mech.* **253**, 105–140.

Sarpkaya, T. 1995 Turbulent vortex breakdown. *Phys. Fluids* **7**, 2301–2303.

Sarpkaya, T. 2002 Experiments on the stability of sinusoidal flow over a circular cylinder. *J. Fluid Mech.* **457**, 157–180.

Sarpkaya, T. 2004 A critical review of the intrinsic nature of vortex-induced vibrations. *J. Fluids Struct.* **19,** 389–447.

Sarpkaya, T. & Butterworth, W. 1992 Separation points on a cylinder in oscillating flow. *Trans. ASME*: *J. Offshore Mech. Arctic Engng* **114**, 28–35.

Schlichting, H. 1932 Berechnung ebener periodischer Grenzschichtströmungen. *Phys. Z.* **33**, 327–335.

Schlichting, H. 1979 *Boundary-Layer Theory*, p. 428. McGraw-Hill.

Sears, W. R. 1956 Some recent developments in airfoil theory. *J. Aerospace Sci.* **23**, 490–499.

Smith, C. R. & Walker, J. D. A. 1995 Turbulent wall-layer vortices. In *Fluid Vortices* (ed. S. I. Green), pp. 235–290. Kluwer.

Stokes, G. G. 1851 On the effect of the internal friction of fluids on the motion of pendulums. *Trans. Camb. Phil. Soc.* **9**, II, 8–106 or *Collected Papers*, vol. III, p.55.

Taneda, S. 1980 Definition of Separation. *Rep. Res. Inst. Appl. Mech. Kyushu University* **28**, 73–81.

Van Dommelen, L. L. & Shen, S. F. 1982 The genesis of separation. In *Numerical and Physical Aspects of Aerodynamic Flows* (ed. T. Cebeci), pp. 293–311. Springer.

WALKER, J. D. A. 2003 Unsteady separation processes at high Reynolds number and their control. *Proc. IUTAM-2002 on Unsteady Separated Flows, Toulouse*, pp. 1–12.

WILLIAMS, J. C. 1977 Incompressible boundary layer separation. *Annu. Rev. Fluid Mech.* **9**, 113–144.

WISSINK, J. G. & RODI, W. 2003 DNS of a laminar separation bubble in the presence of oscillating external flow. *Flow, Turbulence Combust.* **71**, 311–331.

ZDRAVKOVICH, M. M. 1997 *Flow Around Circular Cylinders*, vol. 1: *Fundamentals*. Oxford University Press.

ZDRAVKOVICH, M. M. 2003 *Flow Around Circular Cylinders*, vol. 2: *Applications*. Oxford University Press.

ZDRAVKOVICH, M. M. 2006 *Flow Around Circular Cylinders*, vol. 3: *Unsteady Flows*. Oxford University Press (in press).